analytical chemistry

Article

Cite This: *Anal. Chem.* 2018, 90, 3045−3049

pubs.acs.org/ac

Surface Interrogation Scanning Electrochemical Microscopy for a Photoelectrochemical Reaction: Water Oxidation on a Hematite Surface

Jae Young Kim,[†,‡] Hyun S. Ahn,[*,§] and Allen J. Bard[*,†]

[†]Center for Electrochemistry, Department of Chemistry, The University of Texas at Austin, Austin, Texas 78712, United States

[‡]Korea Research Institute of Chemical Technology, 141 Gajeong-ro, Yuseong-gu, Daejeon 34114, Republic of Korea

[§]Department of Chemistry, Yonsei University, 50 Yonsei-ro, Seodaemun-gu, Seoul 03722, Republic of Korea

Supporting Information

ABSTRACT: To understand the pathway of a photoelectrochemical (PEC) reaction, quantitative knowledge of reaction intermediates is important. We describe here surface interrogation scanning electrochemical microscopy for this purpose (PEC SI-SECM), where a light pulse to a photoactive semiconductor film at a given potential generates intermediates that are then analyzed by a tip generated titrant at known times after the light pulse. The improvements were demonstrated for photoelectrochemical water oxidation (oxygen evolution) reaction on a hematite surface. The density of photoactive sites, proposed to be Fe^{4+} species, on a hematite surface was successfully quantified, and the photoelectrochemical water oxidation reaction dynamics were elucidated by time-dependent redox titration experiments. The new configuration of PEC SI-SECM should find expanded usage to understand and investigate more complicated PEC reactions with other materials.

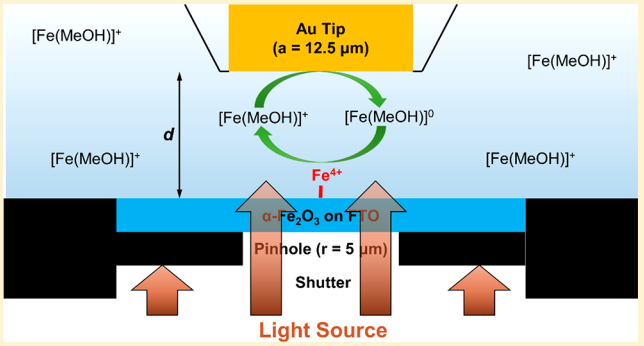

Surface interrogation scanning electrochemical microscopy (SI-SECM) is an effective technique for the analysis of surface dynamics in situ, selectively at the solution−electrode interface.[1,2] Several recent studies utilizing SI-SECM have been particularly valuable in interrogating catalyst surfaces for reactions pertaining to renewable energy (e.g., the oxygen evolution reaction (OER[2−4]) and that for hydrogen (HER[5,6])), thereby advancing the understandings of the reaction mechanism and the nature of the active species. Water oxidation reaction has attracted significant attention as one of important reactions in solar energy applications;[7−9] however, most administrations of SI-SECM toward water oxidation were performed under dark conditions. Due to several technical challenges, progress of SI-SECM research for photoelectrochemical catalysts was slow over the past decade; however, meaningful improvements were made employing back-illumination LEDs[10,11] or an inverted microscope.[12] In addition to this, the scope of interrogated surfaces has extended to include $SrTiO_3$,[13−15] Mo:$BiVO_4$,[16] p-type Cu_2O,[17] and CdSe/CdS quantum rods[18] for the OER. In large band gap semiconductors, such as TiO_2 and $SrTiO_3$, irradiation produces hydroxyl radical leading to O_2 directly (Figure 1A),[19] although adding a dark OER catalyst can improve the efficiency. For smaller band gap materials, for example, Fe_2O_3, as discussed here, the metal ion serves as the means for oxygen evolution (Figure 1B).[20,21]

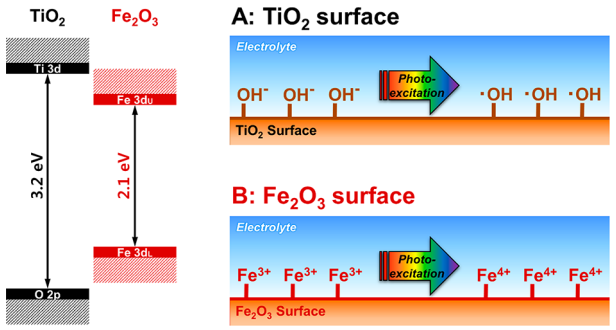

Figure 1. (Left) Band structures for TiO_2 and Fe_2O_3: the band gaps are 3.2 and 2.1 eV, respectively. The valence band edge predominantly consists of O 2p level for TiO_2, while that of Fe_2O_3 is composed of Fe $3d_U$ level for Fe_2O_3 (Fe 3d level splits in the two levels: Fe $3d_L$ (lower) and Fe $3d_U$ (upper) levels due to the octahedral coordination of oxygen around Fe).[19−21] (Right) Under irradiation, the TiO_2 surface forms OH radicals via the contribution of the O 2p orbitals near the valence band minima.[19] On the other hand, the oxidation state of Fe changes to Fe^{4+} for Fe_2O_3 surface because the valence band edge of Fe_2O_3 consists of Fe $3d_U$.[20,21]

Received: November 15, 2017
Accepted: February 2, 2018
Published: February 2, 2018

DOI: 10.1021/acs.analchem.7b04728
Anal. Chem. 2018, 90, 3045−3049

In the present study, we describe a newly developed configuration of SI-SECM for the analysis of photoelectrochemical reactions (Scheme 1). The improved parts for more accurate analysis are (1) light irradiates the substrate electrode from the bottom while the tip electrode is placed above the substrate electrode so that the light reaches the substrate electrode without interruption, (2) the photoactive area of the substrate electrode to be analyzed is better controlled and defined with a small light spot irradiation, (3) a light-shutter system controls the irradiation time with high precision and good resolution (~ms). All the improvements collectively increase the collection efficiency (explained in detail in the Results and Discussion) of the SI-SECM setup for photoelectrochemical (PEC) reactions to better analyze surface dynamics.

Scheme 1. New Configuration of Surface Interrogation Scanning Electrochemical Microscopy (SI-SECM) Setup to Analyze Photoelectrochemical Reactions[a]

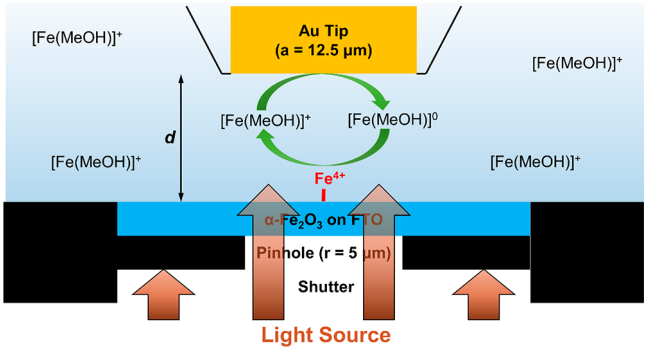

[a]Improvements over the conventional setups are, first, light irradiates the substrate electrode from the bottom, while the tip electrode is placed above the substrate electrode so that the light reaches the substrate electrode without interruption; second, the photoactive area of the substrate electrode to be analyzed is better controlled with a small light spot irradiation; and last, a light-shutter system controls the irradiation time with high precision and good resolution (~ms).

Water oxidation on a hematite (α-Fe_2O_3) surface was selected as a reaction to be analyzed with the PEC SI-SECM setup. Unlike TiO_2[15,22] and $BiVO_4$,[16] which have been investigated several times with SI-SECM as photocatalysts for water oxidation, α-Fe_2O_3 has never been investigated with SI-SECM. Iron species are interesting because they play roles as an electrocatalyst and a photocatalyst simultaneously.[23,24] In the present study, a hematite thin film electrode was employed as a substrate electrode of PEC SI-SECM. As light irradiated the hematite thin film, the photoexcited iron species (likely Fe^{4+}) were generated on the surface of the thin film and were quantitatively titrated by a solvated redox mediator.

EXPERIMENTAL SECTION

An ultramicroelectrode (UME, a = 12.5 μm, RG = 3) was fabricated with gold wire (99.99+%, Goodfellow, Devon, PA) and used as a tip electrode of SI-SECM. The fabrication method is described elsewhere.[2] The surface of the electrode was polished with alumina paste on microcloth pads and cleaned with deionized water prior to use. The hematite (α-Fe_2O_3) thin film was synthesized on F-doped tin oxide (FTO) coated glass and used as a substrate electrode of SI-SECM. The synthesis method is described elsewhere.[24] Briefly, the starting material (β-FeOOH) was grown on FTO coated glass at 100 °C for 6 h in an aqueous solution containing Fe precursor (0.15 M $FeCl_3 \cdot 6H_2O$) and 1 M $NaNO_3$. The resultant thin film was annealed at 800 °C for 20 min to obtain α-Fe_2O_3. A total of 1 mM aqueous ferrocene methanol ($FcMeOH^0$) solution (0.1 N borate/HCl buffer at pH 9) was pre-electrolyzed to obtain the oxidized form ($FcMeOH^+$) just before the beginning of the experiment. For all electrochemical measurements, a platinum wire and an Ag/AgCl electrode were used as a counter electrode and a reference electrode, respectively.

RESULTS AND DISCUSSION

Electrode Configuration. In a PEC SI-SECM setup, two ultramicroelectrodes (UMEs) of approximately the same size are used as a tip electrode and a substrate electrode. The distance between the two UMEs must be sufficiently small so that the surface-bound analytes generated at the substrate electrode can quantitatively be titrated by redox species generated at the tip electrode. For this study, a gold UME (a = 12.5 μm) was used as the tip electrode. A hematite thin film was used as a substrate electrode and its photoactive area was controlled with a pinhole (radius = 5 μm). The pinhole was placed under the substrate electrode and the penetrating light irradiated the substrate electrode, creating a photoanode area with a diameter of ca. 40 μm (Scheme 1 and inset of Figure S1). Details on approach and alignment of the electrodes are in

Scheme 2. Redox Titration Sequence to Analyze the Photoactive Species on a Hematite (α-Fe_2O_3) Surface[a]

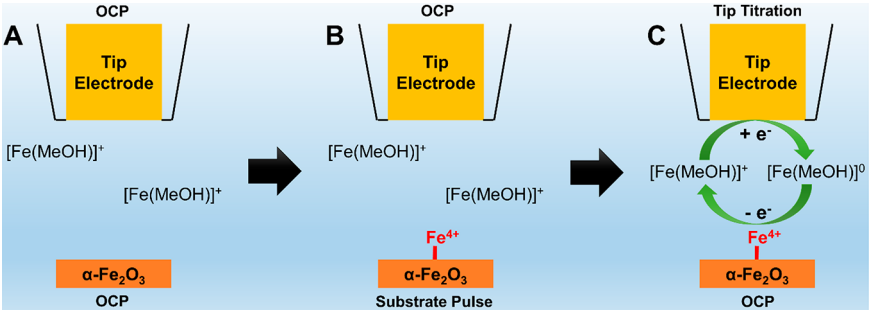

[a](A) Redox mediator is in its oxidized form ($FcMeOH^+$) at the beginning of the experiment. At this stage, no reaction occurs between $FcMeOH^+$ and hematite surface-bound Fe^{3+} species. (B) As light irradiates the substrate along with applied potential, the photoexcited species (likely Fe^{4+}) are generated. (C) After some time delay, the redox mediator is reduced at the tip electrode to generate the titrant ($FcMeOH^0$), which reduces the photoexcited state of the substrate. The resulting feedback current allows for the quantification of the surface-bound excited species concentration.

DOI: 10.1021/acs.analchem.7b04728
Anal. Chem. 2018, 90, 3045−3049

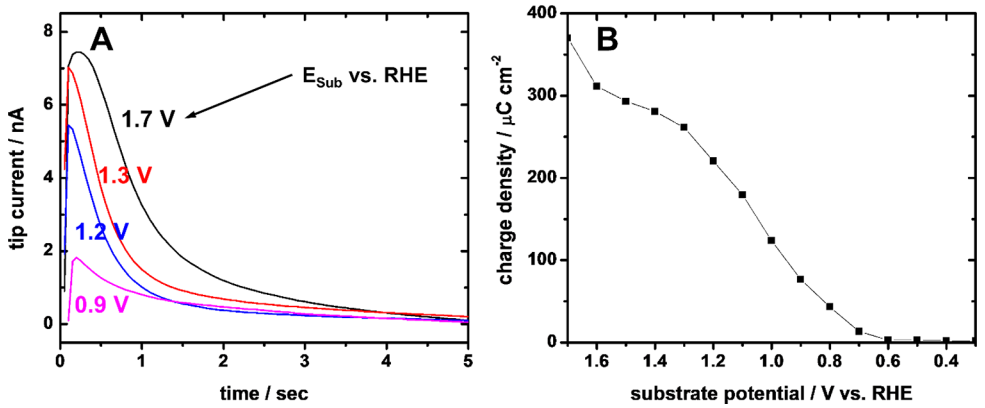

Figure 2. (A) Titration curves (chronoamperograms) of the photoexcited states (Fe^{4+}) on the hematite (α-Fe_2O_3) surface at various substrate potentials (E_{sub}). The tip electrode was pulsed to 0 V vs Ag/AgCl to generate the titrant ($FcMeOH^0$). (B) Currents arising from the reduction of the titrands were integrated to yield charge density (concurrent to the surface-active site density) and are plotted as a function of E_{sub}. Titration experiments were conducted in a 1 mM aqueous $FcMeOH^+$ solution (0.1 N borate/HCl buffer at pH 9).

the Supporting Information. After the approach and alignment, the distance between the tip and the substrate electrodes was 3.8 μm. Ferrocenemethanol ($FcMeOH^{+/0}$, E^0 = 0.44 vs NHE) was used as a redox mediator. The redox mediator solution (0.1 N borate/HCl buffer at pH 9) was pre-electrolyzed before use so that the mediator is in its oxidized form ($FcMeOH^+$) at the beginning of the experiment (Scheme 2A). At this stage, the surface of the substrate electrode contains only Fe^{3+} as its initial state. As light irradiates the substrate at various applied potentials, the photoexcited states (likely Fe^{4+}) are generated due to the transition from Fe^{3+} (Scheme 2B). Unlike the cases of large band gap semiconductors, such as TiO_2 and $SrTiO_3$, higher oxidation state (4+) metal ion serves as the means for oxygen evolution in smaller band gap Fe_2O_3 (Figure 1B).[20] After various time delays (0–5 s), the redox mediator is reduced at the tip electrode to generate the titrant ($FcMeOH^0$), which reduces the photoexcited state of the substrate (Scheme 2C). As a result, the surface photoexcited species of the substrate can quantitatively be titrated with a redox cycle of the mediator. The electrical relays in the device were calibrated in our previous study[25] for the bipotentiostat to control the time during which an electrical signal is applied to the tip or substrate electrode. In this study, the light shutter was further calibrated with chemical actinometry to control the irradiation time of the substrate electrode.[26,27] Potassium ferrioxalate ($K_3[Fe(C_2O_4)]_3$), one of representative chemical actinometers, was used for this purpose (for details, on calibration of the shutter, see the Supporting Information). In short, we were able to control the three time zones using the shutter: during t_1, light irradiates the substrate electrode and the potential is applied to the electrode simultaneously to generate the photoexcited species to be analyzed; there is t_{delay} (time delay) between t_1 and t_2; and during t_2, the titrant is generated at the tip electrode and starts the titration of the photoexcited species on the surface of the substrate electrode. The right-hand side image of Figure S1 is the CVs recorded for the tip and substrate electrodes simultaneously to determine a collection efficiency of the current photo SI-SECM setup. Compared to diffusion limited current of the tip electrode due to the titrant generation, diffusion limited current of the substrate electrode due to the titrant consumption was ca. 87%. It is possibly due to the larger active area of the substrate electrode (diameter = ~40 μm) than that of the tip electrode (diameter = 25 μm) that the titrants reacted with the edge part of the active area of the substrate electrode were lost via diffusion out of the tip–substrate gap. Through our modifications to the photo SI-SECM setup, now the irradiation path is from the bottom of the substrate and, therefore, does not interfere with the electrochemistry at the tip electrode. The application of a pinhole enabled the generation of the photoelectrode (substrate) that is size-comparable to that of the tip (10 s of μms) with precise control. However, further improvements are imaginable with less than unity collection efficiency. Further enhancements to the design are underway: for the purposes of this article, a correction factor to account for the collection efficiency loss (ca. 13%) were placed for our data processing.

Redox Titration of an α-Fe_2O_3 Photoanode. Figure 2A is the titration curve recorded by chronoamperometry (CA) showing shapes similar to those found in our previous SI-SECM studies done in the absence of light. The current at the tip electrode was measured during t_2 by varying the applied potential of the substrate electrode. During the measurement, the potential of the tip electrode was kept at a constant value, 0 V versus Ag/AgCl at which the redox mediator is reduced and generates the titrant ($FcMeOH^0$). The tip current decreases as a function of time due to the consumption of the surface photoexcited species of the substrate electrode. As the substrate potential increases, the tip current also increases representing more positive substrate potentials produce higher concentrations of the surface photoexcited species. The titration curves were integrated to obtain charge density—representative of number of the titrands per geometric electrode area, as shown in Figure 2B. The charge densities in Figure 2B were obtained after background correction to remove currents arising from small amounts of O_2 collection at the tip electrode at high E_{subs} (the amount of collected current due to direct reduction of O_2 can be found in Figure S3). Oxygen collection experiments were separately performed in the absence of the titrant. The increased feedback currents at elevated potentials displayed in Figure 2A are represented as higher charge densities in Figure 2B. The shape of Figure 2B particularly resembles that of the bulk photocurrent–potential curve (Figure S4 in the Supporting Information) of the hematite thin film. We used the same potential range to record the diagrams in Figures 2 and S4 for comparison. An onset potential and a plateau appear at the identical positions for Figures 2B and S4. This resemblance suggests that the surface reactions analyzed by SI-SECM dominate the whole series of processes that generate

DOI: 10.1021/acs.analchem.7b04728
Anal. Chem. 2018, 90, 3045–3049

the bulk photocurrent for the water oxidation reaction on hematite. Density of Fe^{4+} measured by the titration was 18 atoms nm^{-2} (calcd by multiplying the charge density in Figure 2B and 6.24×10^{18} e^-/C, for detailed calculations, see the Supporting Information). The density is reasonable when compared to the known value calculated from crystal packing (ca. 4 atoms nm^{-2}).[28] Higher than expected surface active site density can be attributed to the rough surface morphology of the hematite thin film (substrate electrode). Dimensional fact to note about the hematite film employed here is that the feature size is about 70 nm[29] and the thickness of the thin film is in the order of 500 nm.

Study of OER Kinetics at α-Fe_2O_3 Surface Sites. To elucidate the water oxidation reaction (alternatively, oxygen evolution reaction (OER)) dynamics on the surface of the hematite thin film, a time-dependent titration method was carried out. In the absence of other oxidizable species in the aqueous solution, only water consumes the surface photoexcited species (titrand) of the hematite thin film. Thus, during t_{delay} (time delay between titrand generation and titrant generation), the surface photoexcited species decay via the water oxidation reaction and the subsequent titration current should decrease as a function of the delay time. By varying t_{delay}, the pseudo-first-order OER rate constant of the photoexcited species can be determined (for detailed calculations, see the Supporting Information). Briefly, the titration charge was converted to ln[Fe] and plotted as a function of t_{delay} time (Figure 3), then the rate constant can be obtained from the slope of the plot. The same diagram with Figure 3 but with error bars is displayed in Figure S5. In Figure 3, the results of the time-dependent titration show a linear relationship between ln[Fe] and t_{delay} so that the pseudo-first-order reaction rate constant for OER can be extracted from the plot. The time-dependent studies were performed at two different substrate potentials (E_{sub} = 1.2 and 1.6 V vs RHE: at 1.6 V OER occurs light unassisted, refer to Figure S4). For these potentials, two linear regions were observed and the rate constants for OER were determined as shown in Figure 3. The two linear regions

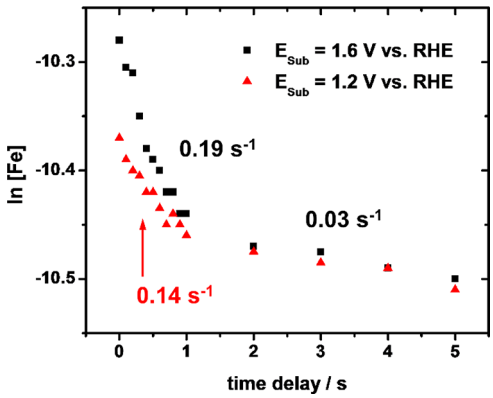

Figure 3. Results of a time-dependent titration of the photoexcited states (Fe^{4+}) on the hematite (α-Fe_2O_3) surface. The titration charge was converted to ln[Fe] and plotted as a function of time delay (t_{delay}). Titration experiments were conducted in a 1 mM aqueous $FcMeOH^+$ solution (0.1 N borate/HCl buffer at pH 9). Pseudo-first order reaction rate constant can be extracted from the slope of the plot according to the equation in the Supporting Information. Error bars were omitted for clarity (the same figure including error bars can be found in Figure S5).

were also reported in our previous study performed for an iron oxide surface as a dark catalyst for OER.[4] It was attributed to the two different mechanisms of OER on iron species which were distinguished as "fast" and "slow" sites. The fractions of "fast" sites were found to be 6.8% and 14.3% respectively for E_{sub} = 1.2 and 1.6 V from Figure 3. These fast site fractions are similar to that of oxygen-deficient iron sites of Fe_2O_3.[30] A similar time dependence was observed in our previous study of a FeOOH catalyst surface.[4] The rate constants for OER on hematite surface were determined as 0.03−0.19 s^{-1} (Figure 3), also similar to those reported in our previous study of the FeOOH surface in the absence of light,[4] indicating that the fundamental surface chemistries are identical both in the presence and in the absence of light, although the applied potentials change due to the added photovoltage for the illuminated system.

Hematite shows unique behavior (multiple linear regions in a time-dependent PEC SI-SECM study) due to its electrocatalytic activity for the OER along with photoelectrocatalytic activity. In another recent study of the OER mechanism on a hematite surface in detail by photoinduced absorption spectroscopy,[20] where one photoexcited hole is related to the rate-determining-step of the OER reported four photoexcited holes involved in OER to form one oxygen molecule. In this case, the rate-determining step is the formation of two oxygen atoms which are connected to the hematite surface with a single covalent bond. The results of the time-dependent titration may reflect several steps with the different reaction rates for OER on a hematite surface.

CONCLUSIONS

A new configuration of the SI-SECM setup to analyze photoelectrochemical reactions has been developed to analyze surface reaction dynamics. Oxygen evolution on hematite surface was selected for analysis with the new setup, making it the first attempt to analyze hematite surface with SI-SECM. In the new configuration, improvements were demonstrated with high collection efficiency (~87%). A hematite thin film was successfully fabricated into a substrate electrode for SI-SECM and analyzed by redox titration. A total of 18 Fe atoms nm^{-2} were detected as photoactive sites on hematite surface by varying the substrate potential. A time-dependent titration was also carried out to elucidate the photoelectrochemical water oxidation reaction dynamics on a hematite surface. By this method, the pseudo-first order reaction rate constants were determined as 0.03 to 0.19 s^{-1}, comparable to that presented in previous studies. The new photo SI-SECM should find broad applications to other photoelectrochemical systems of interest.

ASSOCIATED CONTENT

Supporting Information

The Supporting Information is available free of charge on the ACS Publications website at DOI: 10.1021/acs.analchem.7b04728.

Supplementary data and figures for SI-SECM tip−substrate approach and alignment, shutter calibration with chemical actinometry, calculation of the surface photoactive sites density by titration of $Fe^{4+/3+}$, and measurement of the pseudo-first-order reaction rate constant (PDF).

DOI: 10.1021/acs.analchem.7b04728
Anal. Chem. 2018, 90, 3045−3049

AUTHOR INFORMATION

Corresponding Authors

*Phone: +1-512-471-3761. E-mail: ajbard@mail.utexas.edu.
*Phone: +82-2-2123-2634. E-mail: ahnhs@yonsei.ac.kr.

ORCID

Allen J. Bard: 0000-0002-8517-0230

Notes

The authors declare no competing financial interest.

ACKNOWLEDGMENTS

This work was supported by NSF under the NSF Center for Chemical Innovations (CHE-1305124). H.S.A. was partially supported by Basic Science Research Program through the National Research Foundation (NRF) of Korea funded by the Ministry of Science, ICT and Future Planning (NRF-2017R1C1B2011074), Yonsei University Future-Leading Research Initiative of 2017 (22-0030), and by the Institute for Basic Science (Project Code IBS-R026-D1).

REFERENCES

(1) Rodríguez-López, J.; Alpuche-Avilés, M. A.; Bard, A. J. *J. Am. Chem. Soc.* **2008**, *130*, 16985−16995.
(2) Ahn, H. S.; Bard, A. J. *J. Am. Chem. Soc.* **2015**, *137*, 612−615.
(3) Zoski, C. G. *J. Electrochem. Soc.* **2016**, *163*, H3088−H3100.
(4) Ahn, H. S.; Bard, A. J. *J. Am. Chem. Soc.* **2016**, *138*, 313−318.
(5) Liang, Z.; Ahn, H. S.; Bard, A. J. *J. Am. Chem. Soc.* **2017**, *139*, 4854−4858.
(6) Ahn, H. S.; Bard, A. J. *J. Phys. Chem. Lett.* **2016**, *7*, 2748−2752.
(7) Tachibana, Y.; Vayssieres, L.; Durrant, J. R. *Nat. Photonics* **2012**, *6*, 511−518.
(8) Walter, M. G.; Warren, E. L.; McKone, J. R.; Boettcher, S. W.; Mi, Q.; Santori, E. A.; Lewis, N. S. *Chem. Rev.* **2010**, *110*, 6446−6473.
(9) Sivula, K.; Le Formal, F.; Grätzel, M. *ChemSusChem* **2011**, *4*, 432−449.
(10) Shen, Y.; Nonomura, K.; Schlettwein, D.; Zhao, C.; Wittstock, G. *Chem. - Eur. J.* **2006**, *12*, 5832−5839.
(11) Zhang, B.; Xu, X.; Zhang, X.; Huang, D.; Li, S.; Zhang, Y.; Zhan, F.; Deng, M.; He, Y.; Chen, W.; Shen, Y.; Wang, M. *ChemPhysChem* **2014**, *15*, 1182−1189.
(12) Zhou, X.; Gossage, Z. T.; Simpson, B. H.; Hui, J.; Barton, Z. J.; Rodríguez-López, J. *ACS Nano* **2016**, *10*, 9346−9352.
(13) Simpson, B. H.; Rodríguez-López, J. *J. Am. Chem. Soc.* **2015**, *137*, 14865−14868.
(14) Simpson, B. H.; Rodríguez-López, J. *Electrochim. Acta* **2015**, *179*, 74−83.
(15) Plaza, M.; Huang, X.; Ko, J. Y. P.; Shen, M.; Simpson, B. H.; Rodríguez-López, J.; Ritzert, N. L.; Letchwort-Weaver, K.; Gunceler, D.; Schlom, D. G.; Arias, T. A.; Brock, J. D.; Abruña, H. D. *J. Am. Chem. Soc.* **2016**, *138*, 7816−7819.
(16) Conzuelo, F.; Sliozberg, K.; Gutkowski, R.; Grützke, S.; Nebel, M.; Schuhmann, W. *Anal. Chem.* **2017**, *89*, 1222−1228.
(17) Zhou, J.-H.; Zhao, J.-P.; Wu, L.-K.; Hu, J.-M. *Electrochem. Commun.* **2016**, *72*, 171−175.
(18) Lhenry, S.; Boichard, B.; Leroux, Y. R.; Even-Hernandez, P.; Marchi, V.; Hapiot, P. *Phys. Chem. Chem. Phys.* **2017**, *19*, 4627−4635.
(19) Kakuma, Y.; Nosaka, A. Y.; Nosaka, Y. *Phys. Chem. Chem. Phys.* **2015**, *17*, 18691−18698.
(20) Le Formal, F.; Pastor, E.; Tilley, S. D.; Mesa, C. A.; Pendlebury, S. R.; Grätzel, M.; Durrant, J. R. *J. Am. Chem. Soc.* **2015**, *137*, 6629−6637.
(21) Thimsen, E.; Biswas, S.; Lo, C. S.; Biswas, P. *J. Phys. Chem. C* **2009**, *113*, 2014−2021.
(22) Zhou, X.; Gossage, Z. T.; Simpson, B. H.; Hui, J.; Barton, Z. J.; Rodríguez-López, J. *ACS Nano* **2016**, *10*, 9346−9352.
(23) Chemelewski, W. D.; Lee, H.-C.; Lin, J.-F.; Bard, A. J.; Mullins, C. B. *J. Am. Chem. Soc.* **2014**, *136*, 2843−2850.
(24) Kim, J. Y.; Youn, D. H.; Kang, K.; Lee, J. S. *Angew. Chem., Int. Ed.* **2016**, *55*, 10854−10858.
(25) Ahn, H. S.; Bard, A. J. *Anal. Chem.* **2015**, *87*, 12276−12280.
(26) Ahmed, S. *J. Photochem. Photobiol., A* **2004**, *161*, 151−154.
(27) Fonseca, S. M.; Ahmed, S.; Kemp, T. J.; Unwin, P. R. *Photochem. Photobiol. Sci.* **2003**, *2*, 98−103.
(28) Kiejna, A.; Pabisiak, T. *J. Phys. Chem. C* **2013**, *117*, 24339−24344.
(29) Kim, J. Y.; Youn, D. H.; Kim, J. H.; Kim, H. G.; Lee, J. S. *ACS Appl. Mater. Interfaces* **2015**, *7*, 14123−14129.
(30) Fu, Q.; Li, W.-X.; Yao, Y.; Liu, H.; Su, H.-Y.; Ma, D.; Gu, X.-K.; Chen, L.; Wang, Z.; Zhang, H.; Wang, B.; Bao, X. *Science* **2010**, *328*, 1141−1144.

DOI: 10.1021/acs.analchem.7b04728
Anal. Chem. 2018, 90, 3045−3049